Available online at www.sciencedirect.com

SciVerse ScienceDirect

Ceramics International 39 (2013) 4139–4149

CERAMICS INTERNATIONAL

www.elsevier.com/locate/ceramint

Structure, microstructure and electrical properties of Cu^{2+} doped (K,Na,Li)(Nb,Ta,Sb)O_3 piezoelectric ceramics

F. Rubio-Marcos[a,*], J.J. Reinosa[b], X. Vendrell[c], J.J. Romero[b], L. Mestres[c], P. Leret[b], J.F. Fernández[b], P. Marchet[a]

[a]*Laboratoire de Science des Procédés Céramiques et de Traitements de Surface, UMR 7315 CNRS, Université de Limoges, Centre Européen de la Céramique, 12, rue Atlantis, 87068 Limoges Cedex, France*

[b]*Electroceramic Department, Instituto de Cerámica y Vidrio, CSIC, Kelsen 5, 28049 Madrid, Spain*

[c]*Grup de Química de l'Estat Sòlid, Departament de Química Inorgànica, Universitat de Barcelona, 08028 Barcelona. Spain*

Received 8 October 2012; received in revised form 30 October 2012; accepted 31 October 2012
Available online 13 November 2012

Abstract

This work studies the effects of copper doping on the properties of the $(K_{0.44}Na_{0.52}Li_{0.04})(Nb_{0.86}Ta_{0.10}Sb_{0.04})O_3$ piezoelectric ceramic material. Cu^{2+} incorporation into the perovskite structure produces a transformation of the crystalline lattice from tetragonal to orthorhombic symmetry together with an increase of the secondary phase. The grain size of the ceramic samples is increased due to the formation of a liquid phase during sintering, which increases with the Cu^{2+} content. EDS analysis reveals that the secondary-phase regions present a Cu and Nb-rich composition, indicating that the Cu-excess accommodates through the formation of this secondary phase. Cu-doping induces a rapid increase of the orthorhombic–tetragonal phase transition temperature, while the tetragonal–cubic phase transition temperature is decreased, the latter becoming more diffuse with the increase of Cu content. The piezoelectric properties of the material are reduced with the copper concentration, whereas the mechanical quality factor increases by a factor of nearly four.

Keywords: B. X-ray methods; C. Ferroelectric properties; C. Piezoelectricity; D. Niobates

1. Introduction

Exceptionally high piezoelectric properties were reported for the (K,Na)NbO_3–$LiTaO_3$–$LiSbO_3$ system by Saito et al. in 2004 [1]. This pioneering study was based on chemical modifications in the vicinity of the morphotropic phase boundary (MPB) of $(K_{0.5}Na_{0.5})NbO_3$, (KNN hereafter), by complex simultaneous substitutions in the A (Li) and B (Ta and Sb) sites of the perovskite lattice. Piezoelectric coefficient, d_{33}, over 400 pC/N was reported for textured ceramics prepared by a complex processing method. Some interesting properties were also reported by the same authors [1], for samples elaborated by a conventional ceramic route, particularly for the composition $(K_{0.44}Na_{0.52}Li_{0.04})(Nb_{0.86}Ta_{0.10}Sb_{0.04})O_3$ (Saito's LF4 composition, KNL–NTS hereafter) [$T_c \approx 250$ °C, $d_{33} \approx 300$ pC/N].

The modified KNN ceramics seem to be a suitable substitute for lead zirconium titanate $PbZr_{(1-x)}Ti_xO_3$ (PZT hereafter), the most widely used piezoelectric materials at the present time. In a previous study concerning the KNL–NTS compounds, we have demonstrated that their dielectric, piezoelectric and elastic responses are fundamentally related to extrinsic effects [2]. The dielectric and mechanical losses at room temperature are similar to those of a soft PZT ceramic and too high to be used in power devices. As a consequence, doping has become a very active research field in order to minimize the temperature sensitivity, reduce the dielectric losses and enhance the mechanical quality factor (Q_m) of these materials. Previous researches revealed that high Q_m can be obtained in KNN-based piezoceramics doped with $K_{5.4}Cu_{1.3}Ta_{10}O_{29}$ [3], NiO [4], CoO [5], MnO [6], ZnO [7], $CuNb_2O_6$ [8], or CuO. Moreover, CuO itself is a good sintering aid and it is also

*Corresponding author. Present address: Electroceramic Department, Instituto de Cerámica y Vidrio, CSIC, Kelsen 5, 28049 Madrid, Spain. Tel./fax: +34 917355840.
E-mail address: frmarcos@icv.csic.es (F. Rubio-Marcos).

0272-8842/$ - see front matter © 2012 Elsevier Ltd and Techna Group S.r.l. All rights reserved.
http://dx.doi.org/10.1016/j.ceramint.2012.10.270

used to improve the microstructure texturing and mechanical quality factor [9–14]. Nevertheless, there are still some structural and electrical aspects that remain controversial with respect to the role of dopants in this system, since the published studies mainly concern compositions for which CuO is introduced as a sintering aid, with no substitution for A or B cations involved in the Saito's LF4 composition [12].

In previous works, we studied the effects of different doping elements (Mn^{2+}, Ni^{2+} and Co^{2+}) on KNL–NTS piezoceramics [4–6]. In the present study, Cu^{2+} was selected as the dopant of KNL–NTS ceramics. Considering its ionic radius, Cu^{2+} (r_{Cu}^{2+}: 0.73 Å for a coordination number CN = 6 [15]) falls in the size range of B-site position (r_{Nb}^{5+}: 0.64 Å, r_{Ta}^{5+}: 0.64 Å, r_{Sb}^{5+}: 0.60 Å CN = 6) and to a lower degree of A-site (r_{K}^{+}: 1.64 Å, r_{Na}^{+}: 1.39 Å, r_{Li}^{+}: 0.90 Å, CN = 12). Thus, on the basis of ionic radii, Cu^{2+} could substitute in either A or B-sites [9,12], the most probable position being the B-site from crystal-chemistry considerations, although its real place in the perovskite lattice is disputable. Therefore, based on our previous studies, we selected an A-deficient stoichiometry in order to try to introduce the Cu^{2+} ion in the A-site of the perovskite lattice. The global formula of our samples is $(K_{0.44}Na_{0.52}Li_{0.04})_{(1-x)}Cu_{(x/2)}(Nb_{0.86}Ta_{0.10}Sb_{0.04})O_3$. Such formula considers substitution in A-site of the perovskite lattice, and will then allow comparison with our previous work on Ni^{2+}, Co^{2+} and Mn^{2+} doping [4–6]. The effects of such Cu^{2+} substitution on the phase composition, lattice symmetry and parameters, microstructure, dielectric and piezoelectric properties of $(K_{0.44}Na_{0.52}Li_{0.04})_{(1-x)}Cu_{(x/2)}(Nb_{0.86}Ta_{0.10}Sb_{0.04})O_3$ ceramics are investigated and discussed.

2. Experimental details

The $(K_{0.44}Na_{0.52}Li_{0.04})_{(1-x)}Cu_{(x/2)}(Nb_{0.86}Ta_{0.10}Sb_{0.04})O_3$ compositions with $x = 0.00$, 0.005, 0.01, 0.03 and 0.05, hereafter abbreviated as $(KNL)_{1-x}Cu_{x/2}$–NTS, were synthesized by conventional solid-state reaction [16]. The analytical grade raw materials used in this study were K_2CO_3, Na_2CO_3, Li_2CO_3, CuO, Nb_2O_5, Ta_2O_5 and Sb_2O_5. These powders were carefully weighed and then mixed by attrition-milling using ZrO_2 balls in absolute ethanol medium for 3 h, dried and calcined at 700 °C for 2 h. The obtained powders were attrition milled again and cold-isostatically pressed at 200 MPa into disks of 10 mm in diameter and 0.7 mm in thickness. The pellets were finally sintered in air at 1125 °C for 16 h. The density of the sintered samples was measured using the Archimedes method, showing relative densities over 95% of the theoretical one in all the cases.

Crystalline phases were characterized by X-ray diffraction (XRD) (D8 Advance, Bruker, Germany), using Cu K_α radiation, on powders obtained by milling the sintered ceramics. The lattice parameters were refined by global simulation of the full diagram (pattern matching mode, *fullprof* program).

Room temperature XANES spectra were measured at the ESRF SPLINE line (Grenoble, France) at the Cu K-edge in transmission mode. Beam energy was calibrated by the absorption edge of a Cu foil at 8979 eV.

Microstructures were evaluated on polished and thermally etched samples (1000 °C for 5 min) using a field emission scanning electron microscope, FE-SEM (Hitachi *S*-4700, Tokio, Japan), equipped with energy dispersive spectroscopy, EDS. Grain size distributions and the average grain size were measured from the FE-SEM micrographs using an image analysis program (Leica Qwin, Leica Microsystems Ltd, Cambridge, England) considering more than 500 grains in each measurement.

Electrical characterization was carried out with ceramic discs electroded using fired silver paste (700 °C) on both sides. The temperature dependence of the dielectric permittivity was measured using an impedance analyzer (HP4294A, Agilent Technologies Inc., Santa Clara, CA) in the frequency range of 10^2–10^5 Hz and from 30 to 600 °C using a 2 °C/min heating/cooling rate.

Piezoelectric properties were evaluated after a poling process, carried out in a silicone oil bath at 25 °C under a DC electric field of 40 kV/cm during 30 min. The piezoelectric constant d_{33} was measured using a piezo-d_{33} meter (YE2730A d_{33} METER, APC International). The piezoelectric constant d_{31} and the electromechanical coupling factors k_j were determined at room temperature by the resonance/antiresonance method on the basis of IEEE standards [17]. The planar mechanical quality factor, Q_m, which is related to the sharpness of the resonance frequency, was calculated using the formula [18]:

$$Q_m = \frac{f_a^2}{2\pi f_r Z_m C^T}\left(f_a^2 - f_r^2\right) \quad (1)$$

where f_r is the resonance frequency (Hz), f_a the antiresonance frequency (Hz), Z_m the minimum impedance at f_r (ohm), and C^T the mechanically free capacitance at 1 kHz. The electrical properties of the ceramics were averaged measuring more than four samples.

3. Results and discussion

3.1. Structural characterization

Fig. 1(a) displays the XRD patterns of the ceramics with different Cu^{2+} amounts and Fig. 1(b) shows an enlarged view of these patterns. In addition to the perovskite structure, a secondary phase is detected in all the doped samples. This secondary phase could be assigned to $K_4CuNb_8O_{23}$, with tetragonal tungsten–bronze type structure (TTB). Li et al. [12] also reported that this secondary phase is observed in CuO-doped $(K_{0.52}Na_{0.44}Li_{0.04})(Nb_{0.86}Ta_{0.10}Sb_{0.04})O_3$ ceramics (KNL–NTS), using smaller copper oxide amounts introduced together with the other precursors. However, Shao et al. [9], reported the absence of secondary phases in CuO added $(K_{0.4425}Na_{0.52}Li_{0.0375})(Nb_{0.87}Ta_{0.06}Sb_{0.07})O_3$ ceramic, where the copper oxide is

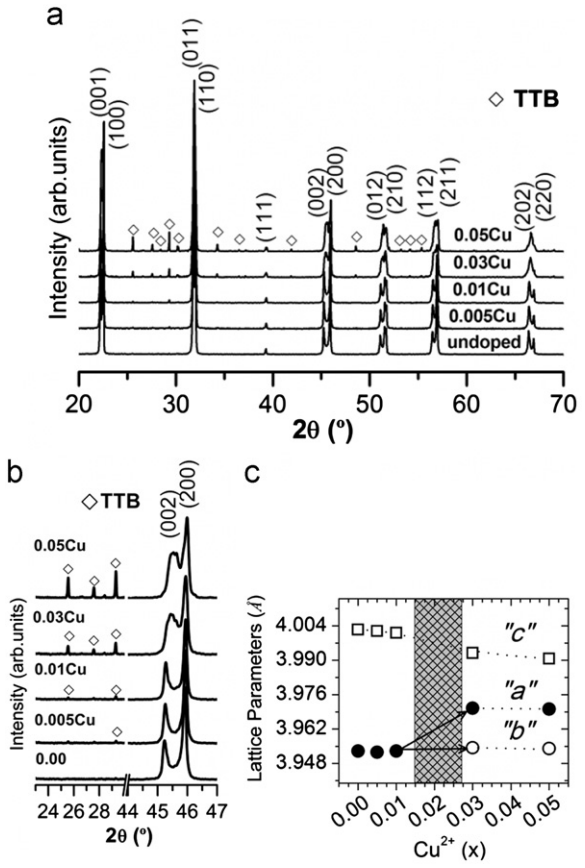

Fig. 1. (a) XRD patterns corresponding to the $(KNL)_{1-x}Cu_{x/2}$–NTS ceramics sintered at 1125 °C for 16 h. (b) Magnified XRD diffraction patterns in the 2θ ranges from 23.5° to 29° and from 44° to 47° of the $(KNL)_{1-x}Cu_{x/2}$–NTS ceramics. (c) Evolution of lattice parameters of the $(KNL)_{1-x}Cu_{x/2}$–NTS ceramics as a function of the Cu^{2+} content.

introduced into the calcined powder before sintering but the occurrence of a small amount of this secondary phase can be detected in their X-ray diffraction patterns. A similar secondary phase was also detected for CuO doping for different compositions [10,14]. Thus, the occurrence of this secondary phase appears as a general tendency for CuO doping for these materials. The disparity in results could be explained by the slight compositional difference, different powder precursors, different processing procedures and different amounts of CuO used. Fig. 1(b) shows a magnification of the XRD patterns in the 2θ ranges from 23.5 ° to 29.0 ° of the $(KNL)_{1-x}Cu_{x/2}$–NTS ceramics, corresponding to the most relevant diffraction peaks of the TTB secondary phase. The results indicate that the TTB content increases, with the increasing Cu^{2+} content, as also observed by Li et al. [12] using smaller copper oxide amounts introduced together with the other precursors. For Li/Ta-modified KNN materials, the TTB secondary phase occurrence was attributed to the volatilization and segregation of the alkali elements during sintering [19], which induces an excess of B-site ions accommodated through the formation of the TTB phase. In our case, the TTB phase probably takes place because of the A-site deficiency introduced by our choice of composition, which corresponds to an excess of B-ions. The Nb^{5+} ions being the most important in the formula, the B-site excess must be compensated by the formation of $K_4CuNb_8O_{23}$ secondary phase. As a consequence, some alkaline deficiency (K,Na,Li) is also expected for the ceramic material since the TTB phase contains such ions.

In order to check the effect of the Cu^{2+} doping on the crystalline structure, the lattice parameters were calculated. As represented in Fig. 1(b), the splitting of the (200) pseudo-cubic peak is modified by Cu^{2+} doping: for the sample without CuO ($x=0.00$), the splitting into (002) and (200) indicates a tetragonal symmetry, while for higher Cu^{2+} contents ($x \geq 0.03$) the (002) peak appears broadened and thus three peaks are observed, which probably implies an orthorhombic symmetry. This behavior, induced by compositional changes, is similar to the temperature induced phase transitions observed for $K_xNa_{(1-x)}NbO_3$ (KNN) around $x=0.5$. For this system, a recent study demonstrated that the symmetry change is difficult to evidence and that the best refinement results were obtained using a monoclinic symmetry with β angle close to 90 [20]. A mixing of the tetragonal and monoclinic symmetries was also observed around the phase transition temperature. In another recent study concerning the phase diagram of KNN [21] around $x=0.5$, the reported space groups were *Pm* (monoclinic) for $x<0.5$ and *Amm2* (orthorhombic) for $x>0.5$ [21] with a progressive change around $x=0.5$. In our case, attempts to perform refinements using a *Amm2* (orthorhombic) or *Pm* (monoclinic) space groups for the highest Cu^{2+} contents ($x \geq 0.03$) were unsuccessful. The best results were obtained using an orthorhombic symmetry and the *P222* (or *Pmmm*) space groups, since this group does not imply any diffraction conditions for Miller indices. As we will report hereafter for the dielectric properties, this inconsistency may arise from the coexistence of two phases, and needs to be further clarified by structural analysis.

The refinement of lattice parameters was thus performed using a tetragonal symmetry for $x<0.03$ (space group P*4mm*) and an orthorhombic one for $x \geq 0.03$ (space group P*222*). Fig. 1(c) shows the evolution of the lattice parameters as a function of the CuO amount. The observed evolution is similar to the one previously evidenced for other doping elements (Mn^{2+}, Co^{2+}, Ni^{2+}) [4–6]. For low Cu^{2+} contents, i.e. the tetragonal range, the lattice parameters remain unchanged, suggesting that the Cu^{2+}-addition does not drastically modify the crystalline structure. A similar evolution was also observed in the same initial composition using low copper oxide amounts [12]. For higher Cu^{2+} contents ($x \geq 0.03$, orthorhombic range, i.e. CuO contents higher than for other studies [12]), the "*c*" lattice parameter decreases slightly with the Cu^{2+} content, while "*a*" and "*b*" increases. So, increasing Cu^{2+} content yields an increase of both the TTB secondary phase and a transformation from tetragonal to orthorhombic symmetry. This evolution clearly depends on the Cu^{2+} content; for low

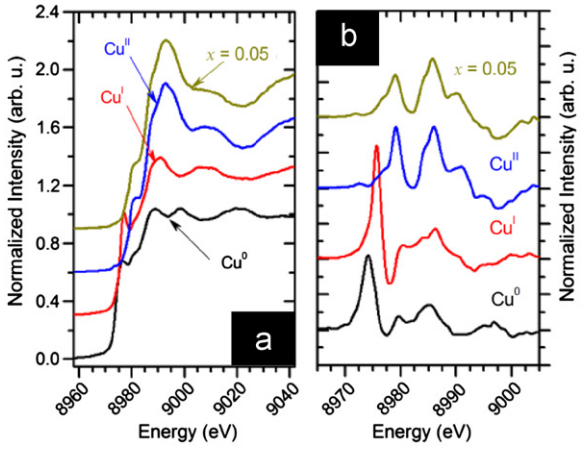

Fig. 2. (a) Room temperature XANES spectra of Cu metal foil, Cu_2O, CuO and composition $x=0.05$ sintered at 1125 °C for 16 h. Part (b) shows the derivative of the XANES spectra.

values of x (tetragonal range) the TTB content increases but the perovskite structure apparently remains unchanged, while for higher values of x (orthorhombic range), the TTB content still increases, together with a structural evolution. Considering the ionic radius of Cu^{2+} (cf. introduction), this behavior is compatible with the hypothesis of the incorporation in A-sites of the perovskite lattice for low doping levels, while higher Cu^{2+} amounts implies incorporation into B-sites, as previously reported [9,12].

In order to check out the oxidation state of copper in the system and to obtain information about its local environment, a XANES study was performed. Fig. 2(a) shows the experimental spectrum of $(KNL)_{1-x}Cu_{x/2}$–NTS for $x=0.05$. In this same figure the XANES spectra of metallic copper, stabilized Cu_2O and CuO (all of them from Aldrich), are included as a reference for comparison purpose. Unfortunately, only the sample with the highest copper content could be measured because of the detection

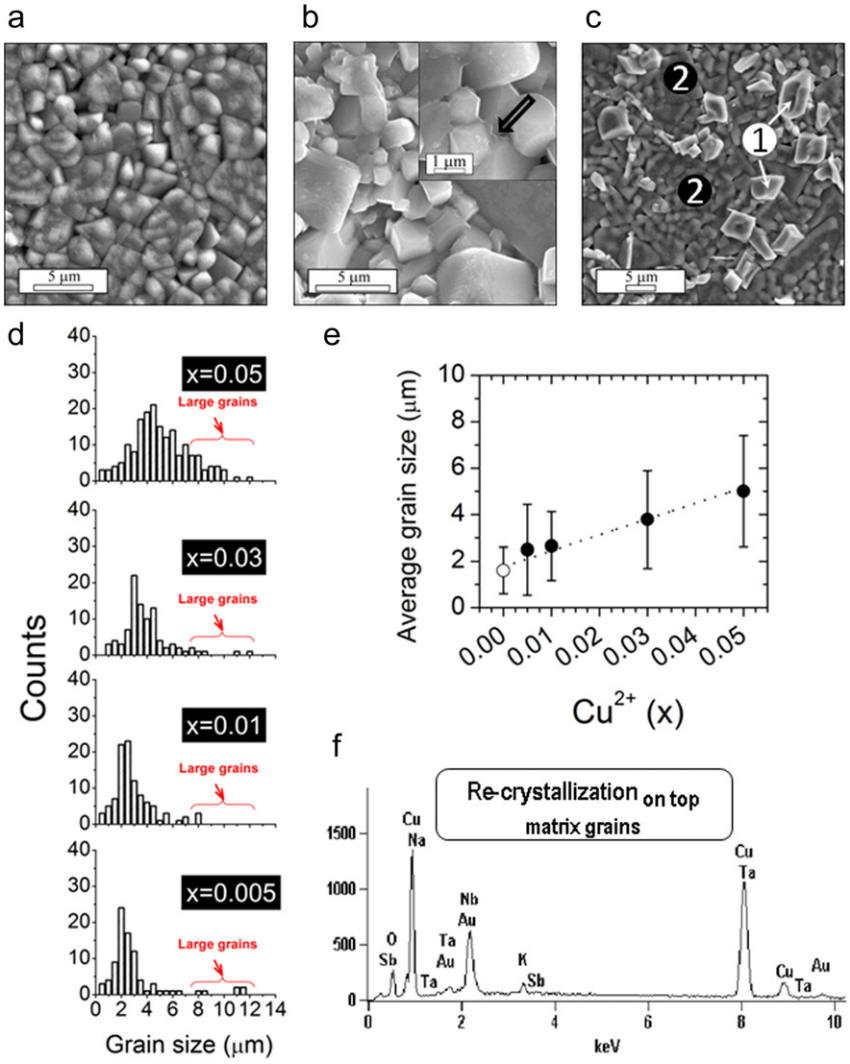

Fig. 3. Microstructure of polished and thermally etched surfaces of the $(KNL)_{1-x}Cu_{x/2}$–NTS ceramics sintered at 1125 °C for 16 h. (a) $x=0.00$, (b) $x=0.01$ and (c) $x=0.05$. Inset of (b) shows a detail of the liquid phase localized at the grain boundaries. In (c), the presence of the secondary re-crystallizations on top the matrix grains and grains with nominal composition corresponds to points 1 and 2 respectively. (d) Grain size distributions of $(KNL)_{1-x}Cu_{x/2}$–NTS samples. (e) Evolution of the average grain size. (d) EDS spectra corresponding to the points marked as 1 in (c).

limits of the equipment. In the other samples, the copper concentration was below this limit and the XANES spectra were too noisy [22]. The XANES spectrum of the sample measured is similar to that of Cu^{2+}, suggesting that the copper oxidation state in the sample is not modified by the calcination and sintering process.

To ensure the results and also to better distinguish the energy at which the absorption edge appears, the derivatives of the XANES spectra are represented in Fig. 2(b). The absorption of Cu^{2+} k-edge XANES is assigned to the main $1s \rightarrow 4s$ transition whereas the next absorption peak corresponds to the $1s \rightarrow 4p$ transition. It is clear that the derivative spectrum for CuO (as Tenorite) and the $(KNL)_{1-x}Cu_{x/2}$–NTS where $x=0.05$ are similar.

Moreover, the similitude of both spectra could indicate that the local symmetry of Cu^{2+} is also similar in both cases. In CuO compound, the Cu^{2+} ions are located at the center of the distorted oxygen octahedra with two different copper–oxygen distances: 1.95 and 1.96 Å [23]. For KNN, Nb atoms are located at the center of oxygen octahedra with a Nb–O distance of 2.00 Å [24]. Since XANES spectrum is very sensitive to the local symmetry of the studied element, the similarity of the observed spectra between our samples and CuO suggests that the Cu^{2+} ions are located in B-site positions, in agreement with X-ray diffraction results for this composition.

3.2. Microstructural characterization

The FE-SEM micrographs of the $(KNL)_{1-x}Cu_{x/2}$–NTS ceramics with $x=0.00$, 0.01, and 0.05 are respectively, shown in Fig. 3(a–c). The microstructure of the sintered samples seems to be very sensitive to Cu^{2+} content. The microstructure of the samples without Cu^{2+}, Fig. 3(a), shows equiaxed grains and some large abnormal square or rectangular grains [7]. A change of the average grain size and grain morphology is observed with Cu^{2+} content, as depicted in Fig. 3(b and c). In addition, for higher Cu^{2+} content ($x \geq 0.03$) secondary re-crystallization begins to appear on top of the matrix grains, see Fig. 3(c).

Grain size distributions of the samples are shown in Fig. 3(d). The arrows indicate the size of the largest grain in each distribution. For x lower than 0.03, the $(KNL)_{1-x}Cu_{x/2}$–NTS system has a narrow unimodal grain size distribution. As Cu^{2+} content increases, the grain size distribution shifts towards larger grain sizes. The addition of the Cu^{2+} causes the grain size distribution to become much broader.

From Fig. 3(e), the evolution of the average grain size can be clearly observed, which increases linearly with the Cu^{2+} content. The average grain size is enhanced from $\sim 1.6 \pm 1.0$ μm in undoped ceramics [7] to $\sim 5.1 \pm 2.4$ μm for the higher Cu^{2+} addition, $x=0.05$.

According to the literature [9,10,12] and to our previous studies [16], the densification of modified KNN ceramics was believed to proceed through the formation of a liquid phase. This liquid phase is localized at grain boundaries, see inset of Fig. 3(b). This liquid phase contributes to sintering by accelerating the particle size redistribution due to the atomic mobility enhancement [25] and therefore, the general grain growth observed in doped samples is also believed to be a result of this liquid phase. Furthermore, the exaggerated grain growth process is driven by the difference in surface free energies between the advancing plane of large grains and the fine matrix grains. The presence of a liquid phase facilitates and accelerates the kinetics of this process, especially in the ceramics with Cu^{2+} content ≥ 0.03. In addition, the grain morphology in these samples changes from sharp-cornered cubical grains with smooth surfaces to cut-cornered grains with rough surfaces, Fig. 3(c), as reported by other authors in CuO-doped KNN-based ceramics [26].

The energy dispersion spectrum analysis (EDS) reveals that the atomic percentages of elements change within the different grain regions, as previously reported for KNN and other systems [26]. Table 1 lists the compositions measured by EDS on the $x=0.05$ sample at the locations marked in Fig. 3(c). The results show clear differences between the different points, indicating a significant compositional segregation in the ceramics. An interesting feature of the $(KNL)_{1-x}Cu_{x/2}$–NTS microstructure is the appearance of secondary re-crystallizations on top of grains, like in Mn-doped samples [6]. The EDS analysis reveals that these large grains have a Cu and Nb-rich composition (see Fig. 3f). This indicates again that the Cu-excess is accommodated through the formation of secondary phases. These re-crystallized grains present irregular morphologies and they can be associated with the TTB secondary phase observed by XRD (points 1, Fig. 3c).

Finally, the matrix grains (point 2, Fig. 3c) have the typical nominal composition with a Na/K concentration ratio around 1.11, slightly lower than the nominal ratio of 1.18 (see Table 1). In addition, traces of Cu can be observed on these grains by EDS, with a Cu content

Table 1
Composition on the points shown on Fig. .3(c) derived from EDS spectra. This table represents the atomic percentages of elements.

	O	Na	K	Li	Cu	Nb	Ta	Sb	Na/K
1 (Secondary phase)	54.12	3.54	1.68	–	33.30	7.05	0.11	0.19	2.11
2 (Matrix)	62.71	7.78	7.00	–	0.40	18.70	2.54	0.93	1.11
KNL-NTS$_{\text{nominal composition}}$	60.00	10.40	8.80	0.80	0.00	17.20	2.00	0.80	1.18
$(KNL)_{1-x}Cu_{x/2}$–NTS ($x=0.05$)	60.00	9.88	8.36	0.76	0.50	17.20	2.00	0.80	1.18

slightly lower than the nominal one. Thus, the solubility of Cu^{2+} in the perovskite lattice appears limited, in agreement with the XRD results.

To sum up, Cu^{2+} doping induces the formation of a liquid phase at the sintering temperature and therefore liquid assisted sintering appears to be the grain consolidation mechanism of the KNL–NTS ceramic. This sintering mechanism usually yields grain growth, as the liquid phase promotes mass transport and enhances densification. However, the crystalline lattice cannot accommodate all Cu^{2+} ions present in the liquid phase and therefore, after the sintering process, the remaining liquid phase re-crystallizes at the grain boundary region as a secondary phase of a structure similar to TTB $K_4CuNb_8O_{23}$.

3.3. Dielectric properties.

Fig. 4 shows the temperature dependence of relative permittivity, ε_r, of $(KNL)_{1-x}Cu_{x/2}$–NTS ceramics at 100 kHz. From Fig. 4(a), two phase transitions are observed at ~25–30 °C and ~310 °C, corresponding, respectively, to orthorhombic–tetragonal (at T_{O-T}) and tetragonal–cubic (at T_c) phase transitions [2]. The T_c decreases with Cu^{2+} content, in contrast to the situation found by Marandian Hagha et al. [26] that reported the insensitivity of Curie temperature for CuO added $(K_{0.44}Na_{0.52}Li_{0.04})(Nb_{0.84}Ta_{0.1}Sb_{0.06})O_3$ composition. However, Li et al. [12] for CuO added $(Na_{0.44}K_{0.52}Li_{0.04})(Nb_{0.86}Ta_{0.1}Sb_{0.04})O_3$ and Alkoy and Papila for CuO added KNN [27] observed a change in T_c with Cu^{2+} addition. Moreover, the addition of CuO produces a slight broadening of the transition peak and the appearance of another anomaly at temperatures close to ~420 °C when the Cu^{2+} amount is ≥ 0.03, thus possibly associated with the TTB secondary phase. For higher Cu^{2+} contents ($x > 0.03$), the dielectric peaks are significantly broadened, suggesting diffuse phase transition characteristics. This result means that the diffuse phase transition is more relevant for the ceramics with a high Cu^{2+} content. This behavior can be induced in many ways, such as by microscopic composition fluctuation, by the merging of micro-domains into macro-domains, or via a coupling of the order parameter and local disorder mode through local strain [28]. For undoped KNL–NTS, Na^+, K^+, and Li^+ ions occupy A sites of the ABO_3 perovskite structure, while Sb^{5+}, Ta^{5+} and Nb^{5+} ions occupy B sites and the phase transition is not diffuse. The diffuse behavior is observed only for CuO-doped KNL–NTS. Thus, one probable origin of this phenomenon is local compositional fluctuations induced by the incorporation of Cu^{2+} ion, whose valence is different from the other ones, into the crystalline lattice of the perovskite compound. Therefore, the increasing cation disorder in the perovskite unit cell could be one of the reasons for the appearance of the diffuse phase transition of the samples with the highest Cu^{2+} content. Furthermore, as mentioned in Figs. 1 and 3, a TTB secondary phase is induced by Cu doping together with some irregular large grain growth. As the Cu^{2+} content increases also does the proportion of these large grains leading to the formation of re-crystallizations on top of the grains. As a consequence, the diffuse phase transition can also be attributed to the microscopic compositional fluctuations intensified by these factors (extrinsic contributions due to the microstructure).

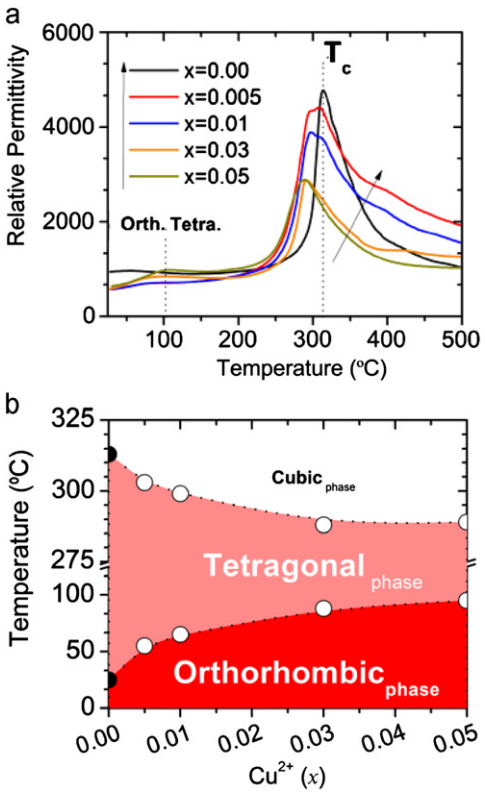

Fig. 4. (a) Temperature dependence of the relative permittivity for $(KNL)_{1-x}Cu_{x/2}$–NTS ceramics with different Cu^{2+} contents. Part (b) shows the evolution of the Curie temperatures T_c and the orthorhombic–tetragonal phase transition temperatures (T_{O-T}) of the $(KNL)_{1-x}Cu_{x/2}$–NTS ceramics with different content in Cu^{2+}. (The sensitivity of the phase transition temperatures, T_{O-T} and T_c, was estimated as ±5 °C).

At the same time, close to room temperature, another anomaly is observed in the dielectric response, Fig. 4(b), identified by a weak maximum in permittivity. As it has been mentioned above, (K,Na)NbO_3-based materials present a phase transition from the orthorhombic to the tetragonal ferroelectric phase, O–T, at temperatures close to ~20 °C [29]. It is also known that in (K,Na,Li)(Nb,Ta)O_3 ceramics, the orthorhombic–tetragonal phase transition temperature, T_{O-T}, decreases as a result of the Li^+ addition, which stabilizes the tetragonal symmetry [30]. The temperature at which this phase transition occurs increases with the Cu^{2+} content, as can be observed in Fig. 4(b). These shifts in the T_{O-T} indicate that the Cu^{2+} incorporation into the perovskite structure produces a stabilization of the orthorhombic symmetry at room temperature, as can be observed by X-ray diffraction (Fig. 1). Moreover, we noticed a peculiar inconsistency between the T_{O-T} values obtained in dielectric measurement and the

actual crystalline structure revealed by XRD (Fig. 1). As observed in Fig. 4(a), all the ceramics (except undoped sample) should be orthorhombic at room temperature, whereas the low Cu^{2+} contents XRD profiles show the tetragonal structure as the main one, as evidenced in Fig. 1. A similar phenomenon has also been observed in the ceramics doped with Li^{+} or Cu^{2+} [9,14,31,32]. The inconsistency may arise from the coexistence of two phases, as indicated by the peak broadening corresponding to T_{O-T}, but needs to be further clarified by structural analysis. Since these compounds include six different cations, the structural resolution appears as very complicated compared to pure' KNN for which the structural resolution is already in progress relatively to the K/Na ratio [20,21].

Fig. 5(a) and (b) represent the room temperature dielectric properties of $(KNL)_{1-x}Cu_{x/2}$–NTS unpoled ceramics at different frequencies (relative permittivity, ε', and dielectric losses, $\tan\delta$). The Cu^{2+} addition globally induces an abrupt decrease of the relative permittivity (Fig. 5c) similar to the one previously observed for the same initial composition using lower copper oxide contents [12]. The evolution is more complicated for the dielectric losses, which are first increased by a factor of three ($x=0.005$) and then decrease quickly down to a value slightly higher to the one of the undoped material (Fig. 5d). The relative permittivity response shows a large frequency range with nearly stable value, in contrast to the situation found in the undoped sample which presents a higher dependency of the relative permittivity versus the frequency, Fig. 5(a). Whatever the origin of such phenomenon, the reduction on the relative permittivity and dielectric losses are favorable results for power applications since it will lower the capacitive effect of the piezoceramic actuators.

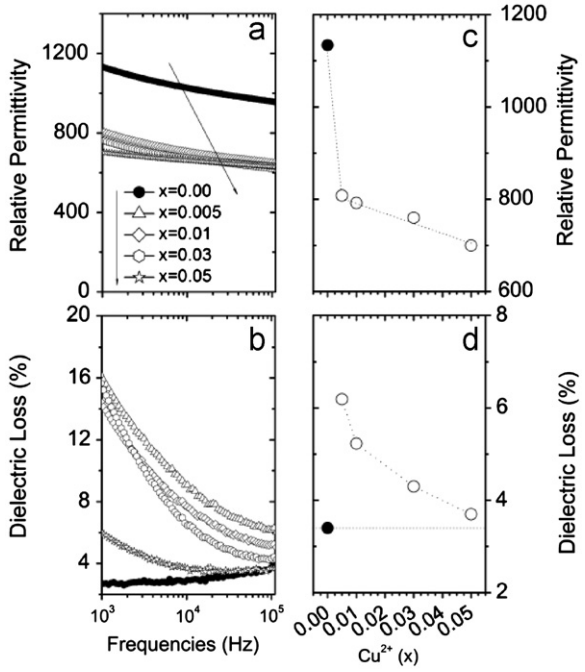

Fig. 5. (a) Relative permittivity and (b) dielectric losses as a function of the frequency for $(KNL)_{1-x}Cu_{x/2}$–NTS ceramics with different Cu^{2+} content. Part (c) shows the evolution of the dielectric constant at 100 kHz in the unpoled ceramics. Part (d) shows the evolution of the dielectric losses at 100 kHz in the unpoled ceramics.

3.4. Piezoelectric properties

Piezoelectric properties (d_j), electromechanical coupling factors (k_j) and mechanical quality factor (Q_m) as a function of the Cu^{2+} content are shown in Fig. 6. The d_{33} decreases slightly for low Cu^{2+} contents ($x \leq 0.01$, the tetragonal range), and then decreases rapidly when x is over 0.03 (orthorhombic range). The same evolution with the Cu^{2+} content was observed in the d_{31} and in the electromechanical coupling factors (k_p and k_t). Generally, both intrinsic and extrinsic effects are involved in such evolution. As we evidenced in a previous study [33], the piezoelectric properties of these materials are mainly modulated by the modification of the lattice distortion induced by the doping element, which reduces the value of the spontaneous polarization as its concentration increases (intrinsic effect).

A high Q_m value is desirable for resonant piezoelectric devices in order to suppress heat generation during the operation of the device [34,35]. In the literature, the Q_m values for undoped KNL–NTS ceramics are reported to be between 30 [35] and 65 [26]. When increasing Cu^{2+} content, the Q_m factor was found to increase from 45 for undoped samples up to a maximum value of 160 for $x=0.05$, see Table 2. The enhancement of the Cu^{2+} doping Q_m values over the undoped Q_m ones is similar to the improvement evidenced in our previous studies for Mn^{2+}, Co^{2+} and Ni^{2+} doping of KNL–NTS [4–6] and by other authors for CuO doping [9,12,26], but the increase is faster than for these other M^{2+} ions. It can be related to the low melting point of CuO that enhances the amount of transient liquid phase and thus promotes the grain growth. This phenomenon leads to an homogeneous microstructure and improves densification of the ceramics (to over 96% theoretical) by a liquid phase mechanism. Therefore, the improvement of Q_m can be mainly attributed to the increased grain size (extrinsic effect) and improved density of the doped samples, [33], since the dielectric losses of doped samples are higher than for undoped ones.

To sum up, the Cu^{2+} incorporation reduces the piezoelectric response, while the mechanical quality factor, Q_m, is increased. As it can be observed from Table 2, Q_m reveals a tendency similar to the one observed in the structure and the piezoelectric properties: low doping levels induces only slight modifications of Q_m and ε_r, while highly doped samples present higher values of Q_m and lower values of ε_r.

3.5. Ferroelectric properties

The ferroelectric loops for the $(KNL)_{1-x}Cu_{x/2}$–NTS ceramics at room temperature are well saturated and the influence of Cu^{2+} in the ferroelectric loops is also evident, see Fig. 7(a–d). As for the structural evolution (XRD,

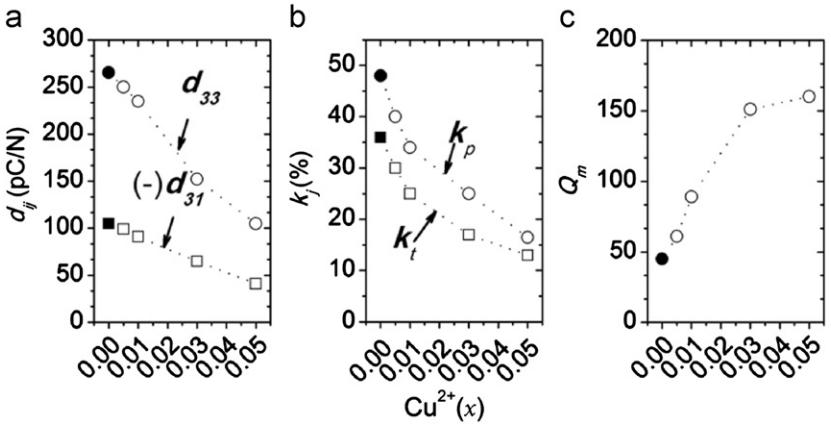

Fig. 6. (a) Variations of the piezoelectric constants, d_{ij}, (b) electromechanical coupling factors, k_j, and (c) planar mechanical quality, Q_m, with the amount of Cu^{2+} in the $(KNL)_{1-x}Cu_{x/2}$–NTS ceramics. Standard tolerances: piezoelectric constant ±5% and mechanical properties ±2.5% (except for Q_m).

Table 2
Summary of the properties of the $(KNL)_{1-x}Cu_{x/2}$-NTS ceramics with different Cu^{2+} content at room temperature. Standard tolerance: Piezoelectric constant ± 5 % (except for Q_m).

	Undoped	**Cu^{2+}**			
x	**0.00**	**0.005**	**0.01**	**0.03**	**0.05**
$\varepsilon_r$at 1 kHz	1134	808	792	760	700
Tan(δ)(%) at 100 kHz	2.7	5.2	5.0	4.1	3.5
d_{33}(pC/N)	265	250	235	152	105
$(-)d_{31}$ (pC/N)	105	99	91	65	41
k_p (%)	48	40	34	25	16
k_t(%)	36	30	25	17	13
Q_m	**45**	**61**	**89**	**151**	**160**

phase transition temperatures and piezoelectric properties), two different ranges can be distinguished from Fig. 7(e and f): when a small amount of Cu^{2+} was added ($x \leq 0.01$), P_r drastically decreases while E_c is increased up to ~17 kV/cm. With further additions of Cu^{2+} ($x > 0.01$), both the P_r and E_c values gradually diminish reaching values from ~18.2 to 8.5 μC/cm^2 and close to 10 kV/cm, respectively. The decrease in P_r indicates that the addition of Cu^{2+} weakens the ferroelectricity of the ceramics. Similar weakening effects have also been reported for other authors in KNN-CuO [9,12,26]. As previously evidenced for Mn^{2+}, Co^{2+} and Ni^{2+} doping of KNL–NTS, this evolution is mainly related to the structural modification induced by doping (intrinsic effect) [33].

4. Discussion

The aim of our work was to incorporate Cu^{2+} ions into the structure of KNL–NTS materials to study the effects of such doping on the structure, phase transition temperatures, dielectric and piezoelectric properties. Contrary to previous works of different authors, which retained a CuO excess added to stoichiometric KNL–NTS composition [9,12,14,26,35], we selected the A-site deficient formula $(K_{0.44}Na_{0.52}Li_{0.04})_{(1-x)}Cu_{(x/2)}(Nb_{0.86}Ta_{0.10}Sb_{0.04})O_3$, in order to introduce the Cu^{2+} ion in the A-site of the perovskite lattice. Indeed, as it has been discussed in the introduction, the most probable position from crystal-chemistry considerations is the B-site, but the incorporation of a limited content of Cu^{2+} in A-sites cannot be excluded. For ferroelectric materials, doping elements can act in various ways: (i) they can be incorporated into the structure, which is thus modified, i.e. intrinsic effects, (ii) they can modify the sintering and grain growth mechanisms, thus changing the microstructure (grain size, morphology) and the ferroelectric domains configuration and size, i.e. extrinsic effects and (iii) they can induce structural defects (like oxygen vacancies) thus modifying the pinning of ferroelectric domains. As a consequence, the role of the doping elements appears as quite complex and must be considered carefully. Nevertheless, we can obtain some conclusions and compare our results to previous works.

When the Cu^{2+} amount is lower than 0.01, the Cu^{2+}-addition does not modify drastically the crystalline structure: the lattice symmetry remains tetragonal with only slight modification of the lattice parameters, but a TTB secondary phase is also generated. It was also confirmed that Cu ions exist in the grains and substitute for A or B-site of the perovskite in the range from 0 to 0.01. The piezoelectric activity is decreased, which confirms a modification of the structure by the doping element. As a logical consequence and similar to our previous results, the explanation of this evolution is that the solubility limit of the doping element is quickly reached and that excess copper ions generate a liquid phase that enhances the diffusion rates and the sintering mechanisms. Meanwhile, a change of the average grain size and grain morphology is also observed. However, the solubility of Cu^{2+} in the perovskite lattice is limited. When the amount of Cu^{2+} is higher than 0.01, the lattice symmetry changes to orthorhombic and the lattice parameters are modified. As a consequence, d_{33} and d_{31} decrease drastically, while Q_m increases (see Table 2). Cu^{2+} ions are supersaturated

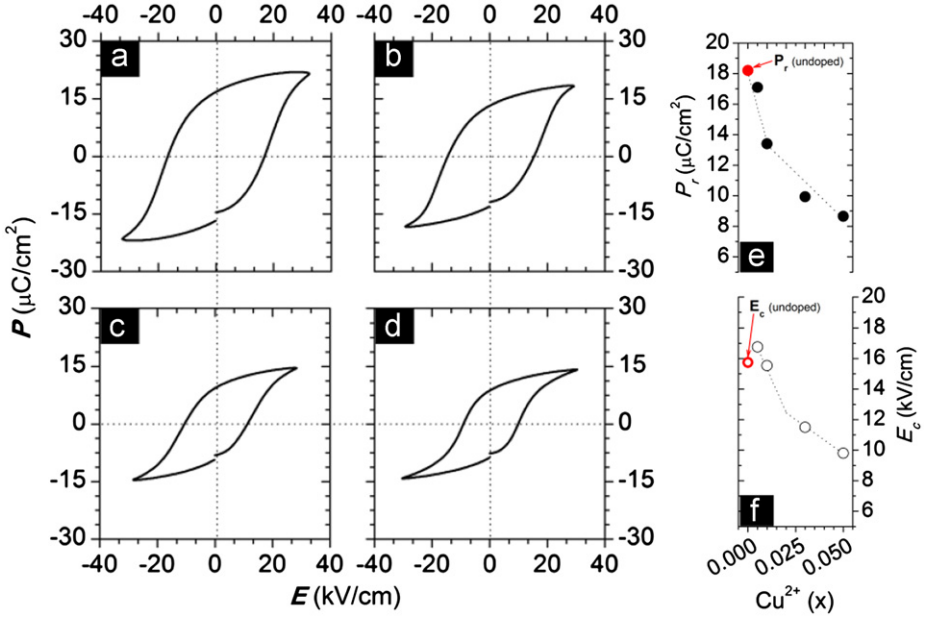

Fig. 7. The polarization-field response of the $(KNL)_{1-x}Cu_{x/2}$–NTS ceramics where (a) $x=0.005$, (b) $x=0.01$, (c) $x=0.03$ and, (d) $x=0.05$. Parts (e) and (f) show the evolution of P_r and E_c on $(KNL)_{1-x}Cu_{x/2}$–NTS ceramics as a function of the x, respectively. The red symbols marked in Fig. 6 (e–f) represent the P_r and E_c values of undoped ceramics, which were previously found to be 18.2 μC/cm^2 and 15.8 kV/cm, respectively.[16].

in the KNL–NTS lattice, and the excess Cu ions enhance the formation of a secondary phase, as evidenced in Figs. 1 and 3(c), resulting in a pinning effect that hinders the motion of ferroelectric domains and then carries the same effect to the piezoelectric properties [36,37].

As we evidenced in a previous study, both intrinsic and extrinsic effects are involved in such evolution [33]. The piezoelectric and ferroelectric properties are mainly modulated by the modification of the lattice distortion induced by the doping element, which reduces the value of the spontaneous polarization (intrinsic effect) as its concentration increase. The reduction of the piezoelectric activity is also correlated to the decrease of relative permittivity, since the piezoelectric coefficient d_{33} is proportional to the spontaneous polarization, P_s, and the dielectric permittivity ε_{33}: $d_{33}=2Q_{11}P_s\varepsilon_{33}$, where Q_{11} is the longitudinal electrostrictive coefficient. Concerning the improvement of Q_m, it can be mainly attributed to the increased grain size and the improvement of the densification induced by the liquid phase generated during sintering (extrinsic effect) [33].

Thus, compared to our previous results for other doping elements (Co^{2+}, Mn^{2+}, Ni^{2+}) [4–6] the solubility limit has the same value, $x=0.01$. This result seems to be similar to the one obtained by other authors for a different initial formula as well: the change from tetragonal to orthorhombic symmetry was not detected by Shao et al. [9] and Li et al. [12] (but the XRD peak splitting is not easy to detect), while Marandian Hagh et al. [26] evidenced the stabilization of the orthorhombic structure ($0<x\leq 1.0$ mol% CuO excess). The TTB secondary phase was only detected by Li et al. [12], but the detection of secondary phases depends on recording and operating conditions of the XRD system. As for our results, Shao et al. [9] and Li et al. [12] also reported unmodified lattice parameters for excess CuO addition lower than one mol% [9] or weight% [12]. However, they describe a more complex evolution for higher CuO contents. As they calculated the lattice parameters using a tetragonal symmetry, the difference observed compared to our results could be due to the fact that they did not detect the orthorhombic splitting.

Considering the phase transition temperatures, some discrepancies are also observed: we evidence a decrease of the Curie temperature, as Li et al. [12], while Marandian Hagh et al. [26] reported the insensitivity of this temperature and Shao et al. [9] reported an increase of this temperature with the CuO content. However, the composition used by these authors is different from the one of the present study, which can explain such difference in the effect of Cu^{2+} doping on phase transition temperatures.

Nevertheless, our results demonstrate an increase of the tetragonal–orthorhombic phase transition temperature, similar to the other reports. The evolution of the piezoelectric properties (d_{ij}, k_j, and Q_m) globally appears similar to the previously published results: the Cu^{2+} doping decreases the piezoelectric activity but the mechanical quality factor Q_m is enhanced. These results are also similar to the ones obtained for other dopants.

5. Conclusions

In conclusion, we demonstrate that Cu^{2+} doping modifies the KNL–NTS structure, giving rise to the appearance of a TTB secondary phase and to changes on the orthorhombic to tetragonal phase transition temperature. The addition of

Cu^{2+} produces a grain size increase, due to the formation of a large amount of liquid phase. The liquid phase excess induces secondary re-crystallizations on top of the grains with a composition rich in Cu^{2+} and Nb^{5+} cations. Finally, a decrease of the piezoelectric coefficient is observed with the added amount of Cu^{2+}. This reduction is probably related to the reduction of the tetragonal phase at room temperature, produced by the increase of the polymorphic phase transition temperature. However, Cu-doping significantly improves the mechanical quality factor (Q_m) of these materials.

Acknowledgments

The authors kindly acknowledge financial support from the MICINN project MAT 2010-21088-C03-01 and COST Action MP0904 SIMUFER. We acknowledge the European Synchrotron Radiation Facility (ESRF) for provision of synchrotron radiation facilities (Project Reference: 25-01-784); beamline 25 (SPLINE). Dr. F. Rubio-Marcos is indebted to the "Conseil Regional du Limousin" for post-doctoral fellowship. Finally, the authors thank C.A. Fernández-Godino for his assistance in the preparation of the compositions.

References

[1] Y. Saito, H. Takao, T. Tani, T. Nonoyama, K. Takatori, T. Homma, T. Nagaya, M. Nakamura, Lead-free piezoceramics, Nature 432 (2004) 84–87.

[2] D.A. Ochoa, J.A. García, R. Pérez, V. Gomis, A. Albareda, F. Rubio-Marcos, J.F. Fernandez, Extrinsic contributions and nonlinear response in lead-free KNN-modified piezoceramics, Journal of Physics D: Applied Physics 42 (2009) 025402.

[3] M. Matsubara, T. Yamaguchi, K. Kikuta, S. Hirano, Synthesis and characterization of $(K_{0.5}Na_{0.5})(Nb_{0.7}Ta_{0.3})O_3$ piezoelectric ceramics sintered with sintering aid $K_{5.4}Cu_{1.3}Ta_{10}O_{29}$, Japanese Journal of Applied Physics 44 (2005) 6618–6623.

[4] F. Rubio-Marcos, P. Marchet, J.J. Romero, J.F. Fernández, Structural, microstructural and electrical properties evolution of $(K,Na,Li)(Nb,Ta,Sb)O_3$ lead-free piezoceramics through NiO doping, Journal of the European Ceramic Society 31 (2011) 2309–2317.

[5] F. Rubio-Marcos, P. Marchet, J.-R. Duclère, J.J. Romero, J.F. Fernández, Evolution of structural and electrical properties of (K, Na, Li)(Nb, Ta, Sb)O_3 lead-free piezoceramics through CoO doping, Solid State Communications 151 (2011) 1463–1466.

[6] F. Rubio-Marcos, P. Marchet, X. Vendrell, L. Mestres, J.J. Romero, F. Rémondiere, J.F. Fernández, Effect of MnO doping on the structure, microstructure and electrical properties of the $(K,Na,Li)(Nb,Ta,Sb)O_3$ lead-free piezoceramics, Journal of Alloys and Compounds 509 (2011) 8804–8811.

[7] F. Rubio-Marcos, M.G. Navarro-Rojero, J.J. Romero, J.F. Fernández, Effect of ZnO on the structure, microstructure and electrical properties of KNN-modified piezoceramics, Journal of the European Ceramic Society 29 (2009) 3045–3052.

[8] M.-R. Yang, S.-Y. Chu, C.-C. Tsai, An ultrasonic therapeutic transducers using lead-free $Na_{0.5}K_{0.5}NbO_3$–$CuNb_2O_6$ ceramics, Journal of Alloys and Compounds 507 (2010) 433–438.

[9] B. Shao, J.-H. Qiu, K.-J. Zhu, Y. Cao, H.-L. Ji, Effect of CuO on dielectric and piezoelectric properties of $(K_{0.4425}Na_{0.52}Li_{0.0375})(Nb_{0.87}Ta_{0.06}Sb_{0.07})O_3$ ceramics, Journal of Alloys and Compounds 515 (2012) 128–133.

[10] M. Matsubara, T. Yamaguchi, W. Sakamoto, K. Kikuta, T. Yogo, S. Hirano, Processing and piezoelectric properties of lead-free $(K,Na)(NbTa)O_3$ ceramics, Journal of the American Ceramic Society 88 (2005) 1190–1196.

[11] H. Takao, Y. Saito, Y. Aoki, K. Hiribuchi, Microstructural evolution of crystalline-oriented $(K_{0.5}Na_{0.5})NbO_3$ piezoelectric ceramics with a sintering aid of CuO, Journal of the American Ceramic Society 89 (2006) 1951–1956.

[12] E. Li, H. Kakemoto, S. Wada, T. Tsurumi, Influence of CuO on the structure and piezoelectric properties of the alkaline niobate-based lead-free ceramics, Journal of the American Ceramic Society 90 (2007) 1787–1791.

[13] D. Lin, K.W. Kwok, H.L.W. Chan, Structure and electrical properties of $K_{0.5}Na_{0.5}NbO_3$–$LiSbO_3$ lead-free piezoelectric ceramics, Journal of Materials Science: Materials in Electronics 21 (2010) 241–245.

[14] B. Shao, J. Qiu, K. Zhu, H. Gu, H. Ji, Influence of sintering temperature on microstructure and electric properties of CuO doped alkaline niobate-based lead-free ceramics, Journal of Materials Science: Materials in Electronics 22 (2012) 1455–1461.

[15] R.D. Shannon, Revised effective ionic radii and systematic studies of interatomie distances in halides and chaleogenides, Acta Crystallographica Section A 32 (1976) 751–767.

[16] F. Rubio-Marcos, P. Ochoa, J.F. Fernández, Sintering and properties of lead-free piezoceramics, Journal of the European Ceramic Society 27 (2007) 4125–4129.

[17] ANSI/IEEE Std 176, in: IEEE Standard on Piezoelectricity, IEEE, USA, 1978.

[18] 〈http://www.ferroperm-piezo.com〉.

[19] Y. Wang, D. Damjanovic, N. Klein, N. Setter, High-temperature instability of Li- and Ta-modified $(K,Na)NbO_3$ piezoceramics, Journal of the American Ceramic Society 91 (2008) 1962–1970.

[20] J. Tellier, B. Malic, B. Dkhil, D. Jenko, J. Cilensek, M. Kosec, Crystal structure and phase transitions of sodium potassium niobate perovskites, Solid State Sciences 11 (2009) 320–324.

[21] D.W. Baker, P.A. Thomas, N. Zhang, A.M. Glazer, A comprehensive study of the phase diagram of $K_xNa_{1-x}NbO_3$, Applied Physics Letters 95 (2009) 091903.

[22] A.I. Frenkel, G.V. Korshin, Studies of Cu(II) in soil by X-ray absorption spectroscopy, Canadian Journal of Soil Science 81 (2001) 271–276.

[23] S. Asbrink, L.J. Norrby, A refinement of the crystal structure of copper(II) oxide with a discussion of some exceptional e.s.d.'s, Acta Crystallographica Section B: Structural Science 26 (1970) 8–15.

[24] A. Kodre, J. Tellier, I. Arčon, B. Malič, M. Kosec, Extended X-ray absorption fine structure study of phase transitions in the piezoelectric perovskite $K_{0.5}Na_{0.5}NbO_3$, Journal of Applied Physics 105 (2009) 113528.

[25] Y. Zhen, J.-F. Li, Abnormal grain growth and new core–shell structure in $(K,Na)NbO_3$-based lead-free piezoelectric ceramics, Journal of the American Ceramic Society 90 (2007) 3496–3502.

[26] N. Marandian Hagh, K. Kerman, B. Jadidian, A. Safari, Dielectric and piezoelectric properties of Cu^{2+}-doped alkali niobates, Journal of the European Ceramic Society 29 (2009) 2325–27332.

[27] E.M. Alkoy, M. Papila, Microstructural features and electrical properties of copper oxide added potassium sodium niobate ceramics, Ceramics International 36 (2010) 1921–1927.

[28] F. Rubio-Marcos, P. Marchet, T. Merle-Méjean, J.F. Fernández, Role of sintering time, crystalline phases and symmetry in the piezoelectric properties of lead-free KNN-modified ceramics (Li/Na/K)(Nb/Ta/Sb)O_3, Materials Chemistry and Physics 123 (2010) 91–97.

[29] B. Jaffe, W.R. Cook, H. Jaffe, in: Piezoelectric Ceramics, Academic, London, 1971.

[30] E. Hollenstein, M. Davis, D. Damjanovic, N. Setter, Piezoelectric properties of Li- and Ta-modified $(K_{0.5}Na_{0.5})NbO_3$ ceramics, Applied Physics Letters 87 (2005) 182905.

[31] X.K. Niu, J.L. Zhang, L. Wu, P. Zheng, M.L. Zhao, C.L. Wang, Crystalline structural phase boundaries in $(K,Na,Li)NbO_3$ ceramics, Solid State Communications 146 (2008) 395–398.

[32] L. Wu, J. Zhang, P. Zheng, C. Wang, Influences of morphotropic phase boundaries on physical properties in (K,Na,Li)$Nb_{0.80}Ta_{0.20}O_3$ ceramics, Journal of Physics D: Applied Physics 40 (2007) 3527–3530.
[33] F. Rubio-Marcos, J.J. Romero, J.F. Fernandez, P. Marchet, Control of the crystalline structure and piezoelectric properties in (K,Na,Li)(Nb,Ta,Sb)O_3 ceramics through transition metal oxides doping, Applied Physics Express 4 (2011) 101501.
[34] M. Matsubara, T. Yamaguchi, K. Kikuta, S. Hirano, Sinterability and piezoelectric properties of (K,Na)NbO_3 ceramics with novel sintering aid, Japanese Journal of Applied Physics 43 (2004) 7159–7163.
[35] E. Li, H. Kakemoto, S. Wada, T. Tsurumi, Enhancement of Q_m by codoping of Li and Cu to potassium sodium niobate lead-free ceramics, IEEE Transactions on Ultrasonics, Ferroelectrics, and Frequency Control 55 (2008) 980–987.
[36] W.L. Zhong, Physics of Ferroelectrics, Science Press, Beijing, China, 1996, pp. 274–285.
[37] T. Kamiya, T. Suzuki, T. Tsurumi, M. Daimon, Effects of manganese addition on piezoelectric properties of $Pb(Zr_{0.5}Ti_{0.5})O_3$, Japanese Journal of Applied Physics 31 (1992) 3058–3060.